AIAA SciTech Forum
4-8 January 2016, San Diego, California, USA
54th AIAA Aerospace Sciences Meeting

AIAA 2016-0261

A study of the grid dependence of the flow field and noise of subsonic jets

Christophe Bogey* and **Olivier Marsden†**

Laboratoire de Mécanique des Fluides et d'Acoustique

UMR CNRS 5509, Ecole Centrale de Lyon

69134 Ecully, France

Three isothermal round jets at a Mach number of 0.9 and a diameter-based Reynolds number of 10^5 are computed by large-eddy simulation using three grids with increasing resolution in order to investigate the grid dependence of the jet flow field and noise. The jets correspond to two initially fully laminar jets and one initially strongly disturbed jet considered in previous numerical studies. At the exit of a pipe nozzle of radius r_0, at $z = 0$, they exhibit laminar boundary-layer mean-velocity profiles of thickness $0.2r_0$, $0.025r_0$ and $0.15r_0$, and peak turbulence intensities close to 0.2%, 0.3% and 9%, respectively. The grids contain up to one billion points, and, compared to the grids used in previous studies, they are much finer in the axial direction for $z \geq 5r_0$, and in the radial direction in the outer region of the jet mixing layers. The main jet flow field and noise characteristics given by the simulations, including the mixing-layer thickness, the centerline mean velocity, the turbulence intensities on the nozzle lip line and the jet axis, velocity spectra in the jets, and near-field and far-field pressure spectra, are presented. For the initially laminar jet with thin boundary layers and the initially disturbed jet, significant differences are found with respect to the results from previous studies. The jet development is more rapid, the turbulence intensities just upstream and downstream of the end of the potential core are higher due to the presence of stronger large-scale structures, and more low-frequency noise is generated. For the three jets, however, the results obtained using the present grids are very similar.

I. Introduction

Since the first developments in the field of computational aeroacoustics in the early nineties,[1] considerable progress has been made in the simulation of the flow and acoustic fields of high-speed turbulent jets,[2–5] which should help us to better describe the underlying noise generation mechanisms. For subsonic jets, in particular, a number of research teams[6–10] have been able to obtain far-field pressure spectra in good agreement with experimental measurements using different numerical methodologies. Nevertheless, for these flows, unlike other flows such as turbulent boundary layers, there is still no clear rule concerning the resolution required to obtain trustworthy solutions. This is due to the fact that even today simulating a jet is difficult and costly, because it has to deal with turbulent flow phenomena whose nature and scales strongly differ. These phenomena take place in the boundary layers in the jet nozzle, in the growing mixing layers, at the end of the potential core located around seven diameters downstream of the nozzle, and in the developed jet region farther downstream. They impose severe and sometimes contradictory constraints on the grid design. Furthermore, some flow phenomena, such as the merging of the mixing layers at the end of the potential core where intense sound sources are found,[11–14] are not very well understood, which makes their calculation uncertain.

In order to validate subsonic jet simulations, the usual approach consists in performing comparisons with experiments. However, these comparisons and their resulting interpretations must be taken with care.

*CNRS Research Scientist, AIAA Senior Member & Associate Fellow, christophe.bogey@ec-lyon.fr
†Assistant Professor at Ecole Centrale de Lyon, olivier.marsden@ec-lyon.fr; currently at the European Centre for Medium-Range Weather Forecasts (ECMWF), Reading, UK

Indeed, the experimental data may be inaccurate due to measurement issues[15] and to acoustic reflections and contaminations.[16,17] For well-known or still-debated reasons, they may also vary significantly from one experiment to another[18–20] Thus, it is fairly easy or, even worse, tempting to choose the sets of data that best match the numerical data to be validated. Among the reasons likely to cause differences between experiments, the effects of the Reynolds number $\mathrm{Re}_D = u_j D/\nu_j$, where $D = 2r_0$ is the jet nozzle diameter, and u_j, and ν_j are the nozzle-exit velocity and kinematic molecular viscosity, and of the initial flow conditions can be emphasized. It has for instance been shown that a Reynolds number $\mathrm{Re}_D \geq 4 \times 10^5$ is required to avoid the effects associated with low Reynolds number.[19] Therefore, the simulations of jets at a low Reynolds number[21–23] should only be compared with experiments at the same Reynolds number, and the simulations of jets at a high Reynolds number may provide irrelevant results if exceedingly dissipative numerical methods are employed. Concerning the influence of the initial conditions, it has been established that more noise is generated in initially laminar jets than in initially turbulent jets, due to the pairings of large coherent structures in the mixing layers of the former jets.[24–28] Consequently, the jet initial conditions in the simulations and the experiments should be identical to carry out meaningful comparisons. Unfortunately, it is rarely feasible due to the limited experimental databases and computational resources available.

Another approach recommended for the validation of simulation accuracy consists in comparing solutions obtained over a range of different grid resolutions in order to demonstrate that the results are grid-independent or grid-convergent. Such studies should be mandatory, but in practice they are very difficult to do because of their prohibitive cost for fully three-dimensional turbulent flows. In these studies, in addition, there is a need to ensure that the solutions are converged in time, and that the initial conditions do not change when the grid is refined, which may not be simple. For subsonic jets at a Mach number of $\mathrm{M} = u_j/c_a = 0.9$, where c_a is the speed of sound in the ambient medium, few grid convergence studies have been conducted. Exceptions include the work by Shur *et al.*,[6,29] Bogey *et al.*,[27,30] Bühler *et al.*[23] and Brès *et al.*[9] In Shur *et al.*,[6] in particular, four grids containing up to 23 million points were considered for a jet at $\mathrm{Re}_D = 1.1 \times 10^6$. Grid independence was not reached, and the finest grid leads to some overestimation of the length of the potential core compared to experiments. In Bogey *et al.*,[30] five grids were used to simulate a jet at $\mathrm{Re}_D = 10^5$ with tripped nozzle-exit boundary layers. The grid resolutions differed mainly in the boundary layers inside the nozzle and in the shear layers just downstream. Hence, the solutions obtained using the fifth grid of 251 millions points were shown to be nearly converged with respect to the grid in the shear layers up to $z = 4r_0$ in the downstream direction, but no solid evidence of their accuracy further downstream was given. This is a pity because in subsonic jets, according to experiments,[31–37] high-frequency sound sources are located near the nozzle exit, whereas low-frequency sources lie farther downstream. In cold jets,[36] for instance, peak source locations are noted around $z = 6r_0$ for Strouhal number $\mathrm{St}_D = fD/u_j = 2$, where f is the frequency, but around $z = 12r_0$ for $\mathrm{St}_D = 0.5$, and $z = 22r_0$ for $\mathrm{St}_D = 0.15$, that is approximately the peak Strouhal number in the spectra measured in the jet direction.[37–39] As a result, the grid resolution in simulations must remain fine enough well beyond the jet potential core.

In the present work, three isothermal round jets at a Mach number of $\mathrm{M} = 0.9$ and a Reynolds number of $\mathrm{Re}_D = 10^5$ are computed by large-eddy simulation (LES) using several grids in order to investigate the grid dependence of the jet flow field and noise. The jets originate at $z = 0$ from a straight pipe nozzle. They correspond to three jets examined in earlier studies,[27,30] namely two initially fully laminar jets with thick and thin nozzle-exit boundary layers, respectively, and an initially strongly disturbed jet in which a forcing is applied to the boundary layers inside the nozzle to generate a high level of turbulent fluctuations at the exit. Three cylindrical grids, containing from 250 million to one billion points, are used. Their resolutions are identical in the upstream boundary layers and in the mixing layers up to $z = 4r_0$, but different in the other flow regions, notably around and downstream of the end of the jet potential core. The results obtained for the three grids are compared between each others, with the results from previous studies using coarser grids, and, for illustration purposes, with experimental data of the literature. The objective of this work is therefore to assess whether the flow and acoustic fields calculated on the present grids have similar features, and to display and quantify their differences with respect to the previous results.

The paper is organized as follows. The main characteristics of the different jets and of the simulations, including inflow conditions, numerical methods, grid and computational parameters, are documented in section II. Vorticity snapshots, nozzle-exit flow velocity profiles, mean and fluctuating velocity profiles obtained along the nozzle lip line and the jet centerline are presented in section III. Pressure snapshots and spectra calculated in the acoustic near field and far field are reported in section IV. Finally, concluding remarks are given in section V.

II. Parameters

A. Jet definition

Three isothermal round jets, referred to as jetv0D0200, jetv0D0025 and jetv9D0150, are simulated. They correspond to jets considered in previously in Bogey and Bailly[27] in the first two cases, and in Bogey *et al.*[30] in the latter case. They have a Mach number of $\mathrm{M} = 0.9$ and a Reynolds number of $\mathrm{Re}_D = 10^5$, as reported in table 1. The ambient temperature and pressure are $T_a = 293$ K and $p_a = 10^5$ Pa. The jets originate at $z = 0$ from a pipe nozzle of radius r_0 and length $2r_0$, whose lip is $0.053r_0$ thick. At the pipe inlet, a Blasius laminar boundary-layer profile of thickness δ_{BL} is imposed for the axial velocity.[27] Radial and azimuthal velocities are set to zero, pressure is equal to p_a, and temperature is determined by a Crocco-Busemann relation.

Table 1. Jet parameters: Mach and Reynolds numbers M and Re_D, thickness of the Blasius laminar boundary-layer profile imposed at the pipe nozzle inlet δ_{BL}, peak turbulence intensity at the nozzle exit u'_e/u_j.

	M	Re_D	δ_{BL}	u'_e/u_j
jetv0D0200	0.9	10^5	$0.200r_0$	0%
jetv0D0025	0.9	10^5	$0.025r_0$	0%
jetv9D0150	0.9	10^5	$0.150r_0$	9%

The three jets are chosen in order to study the grid-independence of the LES results over a wide range of jet initial conditions, which will be later illustrated in section III.A. The boundary-layer thickness δ_{BL} at the pipe nozzle inlet and the peak turbulence intensity u'_e/u_j reached at the exit in the different cases are given in table 1. The first two jets are both initially fully laminar with u'_e/u_j close to 0%, but the boundary layers are thick in jetv0D0200 and thin in jetv0D0025, with $\delta_{BL} = 0.2r_0$ and $\delta_{BL} = 0.025r_0$, respectively. The boundary layers of jetv9D0150 are also rather thick with $\delta_{BL} = 0.15r_0$, but they are tripped in order to generate highly disturbed exit conditions, which would otherwise be laminar, as is usually done in laboratory experiments.[24–26,40] In practice, random low-level vortical disturbances uncorrelated in the azimuthal direction are added at $z = -0.95r_0$ inside the pipe, following the procedure detailed in Bogey *et al.*[30] The forcing strength used in the present simulations is that empirically set in the previous LES[30] of jetv9D0150 to obtain a peak turbulence intensity of 9% at the nozzle exit. Finally, random pressure fluctuations are introduced in the jet shear layers initially at time $t = 0$ in order to reduce the initial transitory period.

B. LES approach and numerical methods

The numerical framework is identical to that used in recent jet simulations,[27,28,30,41–43] including the previous simulations of jetv0D0200, jetv0D0025 and jetv9D0150. The LES are carried out using an in-house solver of the three-dimensional filtered compressible Navier-Stokes equations in cylindrical coordinates (r, θ, z) based on low-dissipation and low-dispersion explicit schemes. The axis singularity is taken into account by the method of Mohseni & Colonius.[44] In order to alleviate the time-step restriction near the cylindrical origin, the derivatives in the azimuthal direction around the axis are calculated at coarser resolutions than permitted by the grid.[45] For the points closest to the jet axis, they are evaluated using n_θ^{axis} points, yielding an effective resolution of $2\pi/n_\theta^{axis}$. Fourth-order eleven-point centered finite differences are used for spatial discretization, and a second-order six-stage Runge-Kutta algorithm is implemented for time integration.[46] A sixth-order eleven-point centered filter[47] is applied explicitly to the flow variables every time step. Non-centered finite differences and filters are also used near the pipe walls and the grid boundaries.[27,48] The radiation conditions of Tam & Dong[49] are applied at the boundaries, with the addition at the outflow of a sponge zone combining grid stretching and Laplacian filtering,[50] to avoid significant acoustic reflections. In the present LES, the explicit filtering is employed to remove grid-to-grid oscillations, but also as a subgrid-scale high-order dissipation model in order to relax turbulent energy from scales at wave numbers close to the grid cut-off wave number while leaving larger scales mostly unaffected. The performance of this LES approach has been assessed in past studies for subsonic jets, Taylor-Green vortices and turbulent channel flows,[30,51–54] from comparisons with solutions of direct numerical simulations and from the examination of the magnitude and the properties of the filtering dissipation in the wavenumber space.

C. Grid parameters

Three cylindrical grids with increasing resolution, referred to as gridz60, gridz47, gridz40, are designed in this study. Their main characteristics are collected in table 2. Those of the grids used in previous simulations[27,30] for jetv0D0200, jetv0D0025 and jetv9D0150, and in a recent study[8] for two jets at $\mathrm{Re}_D = 2\times10^5$, denoted as gridv0D0200old, gridv0D0025old, gridv9D0150old and gridRe2e5, are also given for comparison. The present grids have similar number of points in the radial and axial directions, namely $n_r \simeq 500$ and $n_z \simeq 2000$, and sizes decreasing with the resolution. Thus, the physical extents of gridz60, gridz47 and gridz40 are respectively equal to $L_z = 60r_0$, $47.5r_0$ and $40r_0$ in the axial direction, and to $L_r = 20r_0$, $17r_0$ and $15r_0$ in the radial direction. For all grids, the number of points n_θ in the azimuthal direction can be set to 256, 512 or 1024. Moreover, for stability concerns, the effective number of points n_θ^{axis} close to the jet axis must be reduced to 32 for gridz60 and gridz47, and 16 for gridz40.

Table 2. Parameters of the present grids (gridz60, gridz47 and gridz40) and of grids used in previous studies (gridv0D0200old,[27] gridv0D0025old,[27] gridv9D0150old[28,30,42] and gridRe2e5[8]): numbers of grid points n_r and n_z in the radial and axial directions, effective number of points n_θ^{axis} in the azimuthal direction close to the jet axis, extents of the physical domain L_r and L_z, and mesh spacings Δr and Δz at different positions.

			$\Delta r/r_0$ (%) at $r=$				$\Delta z/r_0$ (%) at $z=$			
	n_r, n_z, n_θ^{axis}	L_r, L_z	0	r_0	$2r_0$	$4r_0$	0	$10r_0$	$20r_0$	$30r_0$
gridz60	512, 1908, 32	$20r_0$, $60r_0$	2.92	0.36	2.93	3.86	0.72	3.11	3.68	4.24
gridz47	499, 1961, 32	$17r_0$, $47.5r_0$	2.03	0.36	2.67	3.61	0.72	2.83	2.83	3.11
gridz40	495, 1977, 16	$15r_0$, $40r_0$	1.89	0.36	2.37	3.31	0.72	2.39	2.39	2.67
gridv0D0200old	173, 502, 8	$8.2r_0$, $20r_0$	2.90	2.90	5.25	5.51	5.80	5.80	5.80	–
gridv0D0025old	287, 651, 8	$8.6r_0$, $25r_0$	2.92	0.36	3.74	5.65	0.72	5.77	5.77	–
gridv9D0150old	249, 962, 16	$6.75r_0$, $25r_0$	2.92	0.36	3.74	8.15	0.72	5.09	6.56	–
gridRe2e5	496, 3052, 32	$8.4r_0$, $28.4r_0$	1.54	0.15	1.83	5	0.31	1.18	2.05	–

The variations of the radial and axial mesh spacings Δr and Δz in the different grids are represented in figures 1 and 2. In order to specify the same initial flow conditions in the previous and present simulations of jetv9D0150 with tripped nozzle-exit boundary layers, the three new grids are derived from gridv9D0150old. More precisely, they are identical to gridv9D0150old for $0.5r_0 \le r \le 1.6r_0$ and $z \le 4r_0$, with mesh spacings $\Delta r = 0.0036r_0$ at $r = r_0$ and $\Delta z = 0.0072r_0$ at $z = 0$ in all cases. Elsewhere, they are similar to or more refined than gridv9D0150old. In the radial direction, the mesh spacings Δr at $r = 0$ and $r = 2r_0$ range from $0.0292r_0$ and $0.0293r_0$ in gridz60 down to $0.0189r_0$ and $0.0236r_0$ in gridz40, whereas they are equal to $0.0292r_0$ and $0.0374r_0$ in gridv9D0150old. The difference in resolution is even more pronounced at $r = 4r_0$, where Δr is found to be $0.0386r_0$ in gridz60 and $0.0815r_0$ in gridv9D0150old, for instance. In the axial direction, the mesh spacings Δz at $z = 10r_0$ and $z = 20r_0$ vary from $0.0311r_0$ and $0.0368r_0$ in gridz60 down to $0.0239r_0$ and $0.0239r_0$ in gridz40, with $\Delta z = 0.0509r_0$ and $0.0656r_0$ in gridv9D0150old. Compared to the previous grids, as also shown in figures 1(c) and 2(c), the present grids are therefore much finer in the radial direction in the outer region of the jet mixing layers, and in the axial direction for $z \ge 5r_0$, notably between $z = 10r_0$ and $z = 25r_0$ where the most significant noise sources of cold jets at M = 0.9 are located according to experimental results.[36] Finally, the maximal mesh spacing in the physical part of the computational domains, for $r \le L_r$ and $z \le L_z$, is equal to $\Delta r = 0.075r_0$, yielding a Strouhal number of $\mathrm{St}_D = 5.9$ for an acoustic wave discretized by five points per wavelength.

D. Simulation parameters

As reported in table 3, each of the three jets in this work is computed using gridz60, gridz47 and gridz40. The time step, defined by $\Delta t = 0.7 \times \Delta r(r = r_0)/c_a$, is the same in the nine cases considered. The grids contain $n_r \times n_\theta \times n_z \simeq 250$ million points for jetv0D0200, 500 million points for jetv0D0025, and one billion points for jetv9D0150, using $n_\theta = 256$, 512 and 1024 points in the azimuthal direction, respectively, depending on the jet initial conditions.[30] As a result, the simulations of the two initially fully laminar jets are faster and could run over a longer period than those of the the tripped jets, providing results better converged in time. For the grids of one billion points, 200 GB of memory are required, and about 1,000 CPU hours are needed for 1,000 iterations using an OpenMP-based in-house solver. Since between 300,000 and 700,000 iterations

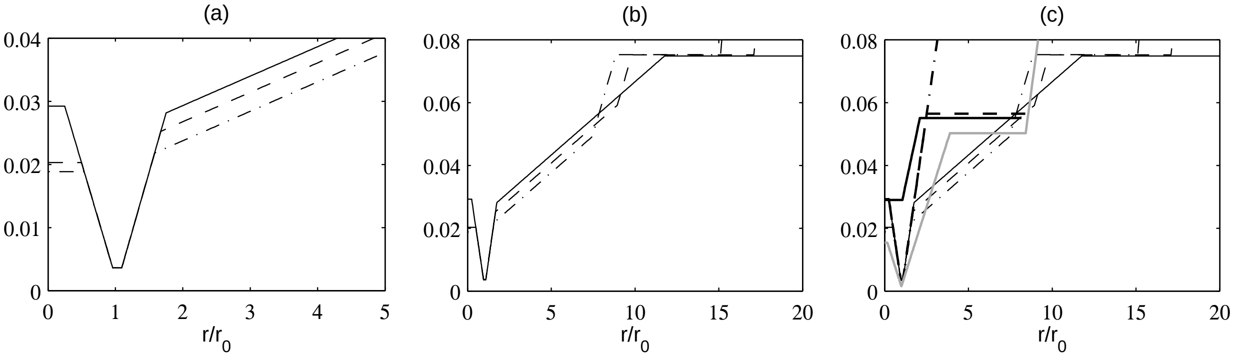

Figure 1. Variations of the radial mesh spacing $\Delta r/r_0$ (a) over $0 \le r \le 5r_0$ and (b,c) over $0 \le r \le 20r_0$ for ——— gridz60, – – – gridz47, – · – · gridz40, ——— gridv0D0200old, – – – gridv0D0025old – · – · gridv9D0150old, and ——— gridRe2e5.

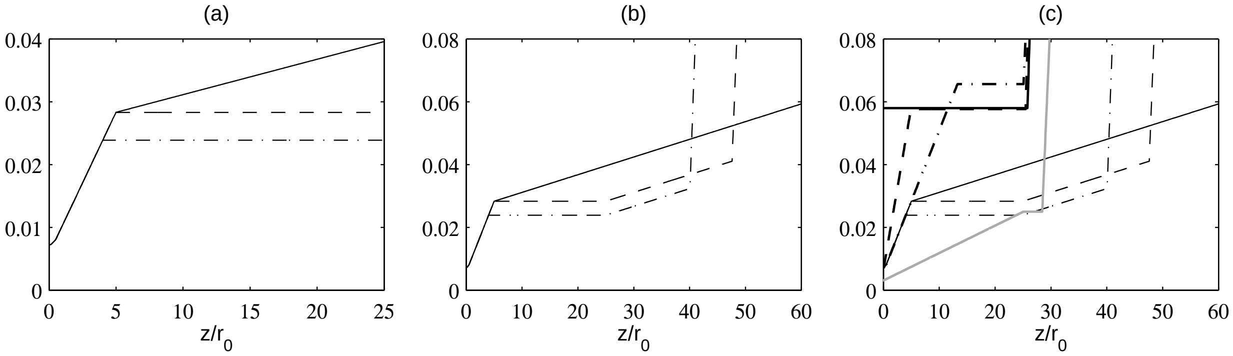

Figure 2. Variations of the axial mesh spacing $\Delta z/r_0$ (a) over $0 \le z \le 25r_0$ and (b,c) over $0 \le z \le 60r_0$ for ——— gridz60, – – – gridz47, – · – · gridz40, ——— gridv0D0200old, – – – gridv0D0025old – · – · gridv9D0150old, and ——— gridRe2e5.

Table 3. Simulation parameters: grids used, number of points in the azimuthal direction n_θ, total number of points, and simulation time T after the transient period.

jet	grid	n_θ	$n_r \times n_\theta \times n_z$	Tu_j/r_0
jetv0D0200	gridz60	256	2.5×10^8	900
jetv0D0200	gridz47	256	2.5×10^8	750
jetv0D0200	gridz40	256	2.5×10^8	600
jetv0D0025	gridz60	512	5×10^8	600
jetv0D0025	gridz47	512	5×10^8	600
jetv0D0025	gridz40	512	5×10^8	600
jetv9D0150	gridz60	1024	10^9	300
jetv9D0150	gridz47	1024	10^9	300
jetv9D0150	gridz40	1024	10^9	300

are performed in each case, a total number of about 2 billion CPU hours is consumed.

The simulation time T after the transient period is equal to $900r_0/u_j$, $750r_0/u_j$ and $600r_0/u_j$ for jetv0D0200 using gridz60, gridz47 and gridz40, respectively, and to $600r_0/u_j$ for jetv0D0025 and $300r_0/u_j$ for jetv9D0150. During that time, density, velocity components and pressure along the jet axis at $r = 0$, and on the surfaces located at $r = r_0$, $r = 15r_0$ and $r = L_r$ and at $z = -1.5r_0$, $z = 0$, $z = 15r_0$, $z = 30r_0$ and $z = L_z$, are recorded at a sampling frequency allowing spectra to be computed up to $\mathrm{St}_D = 12$. Density, velocities and pressure obtained at the azimuthal angles $\theta = 0$, 90^o, 180^o and 270^o are also stored at a halved frequency. The flow and acoustic near field statistics presented in sections III and IV are calculated from these recordings. They are averaged in the azimuthal direction, when possible. Time spectra are evaluated from overlapping samples of duration $45r_0/u_j$ on the jet axis, and $90r_0/u_j$ otherwise. In the azimuthal direction, post-processing can be performed up to the mode $n_\theta = 128$, where n_θ is the dimensionless azimuthal wave number such that $n_\theta = k_\theta r$.

E. Far-field extrapolation

The LES near-field fluctuations are propagated to the acoustic far field using an in-house OpenMP-based solver of the isentropic linearized Euler equations (ILEE) in cylindrical coordinates,[55] as illustrated in figure 3.

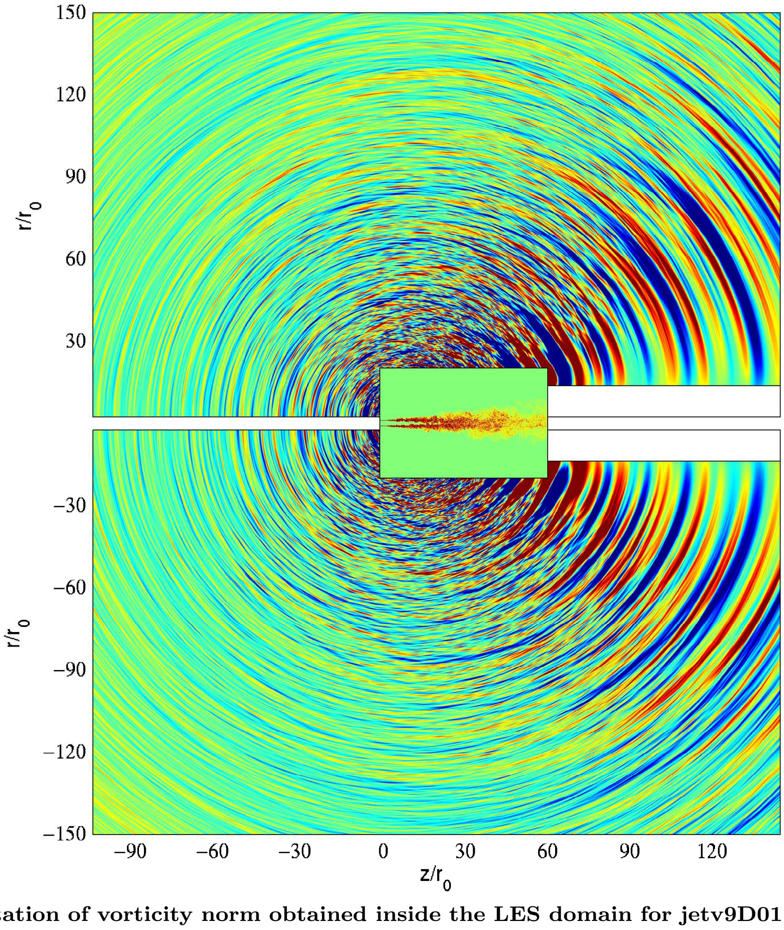

Figure 3. Representation of vorticity norm obtained inside the LES domain for jetv9D0150 using gridz60 and of pressure fluctuations extrapolated outside by solving the ILEE. The color scales range up to the level of $4u_j/r_0$ for vorticity, and from -7 to 7 Pa for pressure.

The extrapolation is performed from the velocity and pressure fluctuations obtained at $z = -1.5r_0$, $r = L_r$ and $z = L_z$ in the jet simulations, recorded over the time periods given in table 3 at a sampling frequency corresponding to $\mathrm{St}_D = 12$. The same numerical methods as in the LES, and a grid containing $n_r \times n_\theta \times n_z = 2048 \times 256 \times 3506 = 1.8$ billion points are used. Excluding the eighty-point sponge zones implemented at the upstream, downstream and outer radial boundaries to minimize acoustic reflections, the grid extends axially from $z = -106r_0$ up to $z = 145r_0$ and radially from $r = 2.5r_0$ up to $r = 151r_0$. In this region, the radial and axial mesh spacings are constant and equal to $\Delta r = \Delta z = 0.075r_0$, yielding $\mathrm{St}_D = 5.9$ for an acoustic wave discretized by five points per wavelength. The near-field fluctuations are interpolated and imposed onto the grid at $z = -1.5r_0$ between $r = 2.5r_0$ and $r = L_r$, at $r = L_r$ between $z = -1.5r_0$ and $z = L_z$, and at $z = L_z$ between $r = r_{min}$ and $r = L_r$, where $r_{min} = 13.85r_0$, $r_{min} = 10.96r_0$ and $r_{min} = 9.23r_0$ for the LES using grid60, grid47 and grid40, respectively. The extrapolation surface is open in the downstream direction, in order to avoid the presence of aerodynamic disturbances,[58] which may cause low-frequency spurious waves as in previous studies.[8,27,30] However, the opening angle relative to the jet direction, with the nozzle exit as an origin, is only $\varphi = 13^{\mathrm{o}}$, which should allow most of the downstream noise components to be taken into account. Each ILEE computation requires 200 GB of memory, and lasts during between 5,000 and 12,000 iterations, resulting to a total number of about 100,000 CPU hours consumed. Pressure is recorded at a distance of $150r_0$ from $z = r = 0$ where far-field acoustic conditions are expected to apply according to measurements,[56,57] as in the experiment of Bridges & Brown,[17] for angles between $\phi = 15^{\mathrm{o}}$ and $\phi = 130^{\mathrm{o}}$. Pressure spectra are evaluated using overlapping samples of duration $90r_0/u_j$, and they are averaged in the azimuthal direction.

III. Jet flow fields

A. Nozzle-exit velocity profiles

The mean and rms axial velocity profiles obtained at the nozzle-exit section of the three jets in the present simulations are presented in figures 4 and 5.

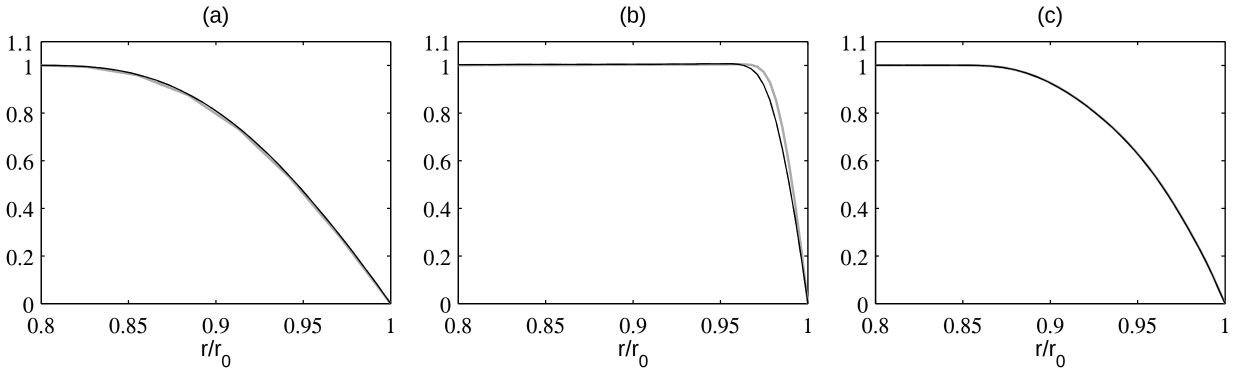

Figure 4. Nozzle-exit radial profiles of mean axial velocity $< u_z > /u_j$ obtained for (a) jetv0D0200, (b) jetv0D0025, and (c) jetv9D0150 using ——— gridz60, – – – gridz47 and – · – · gridz40; ——— results obtained using (a) gridv0D0200old, (b) gridv0D0025old and (c) gridv9D0150old.

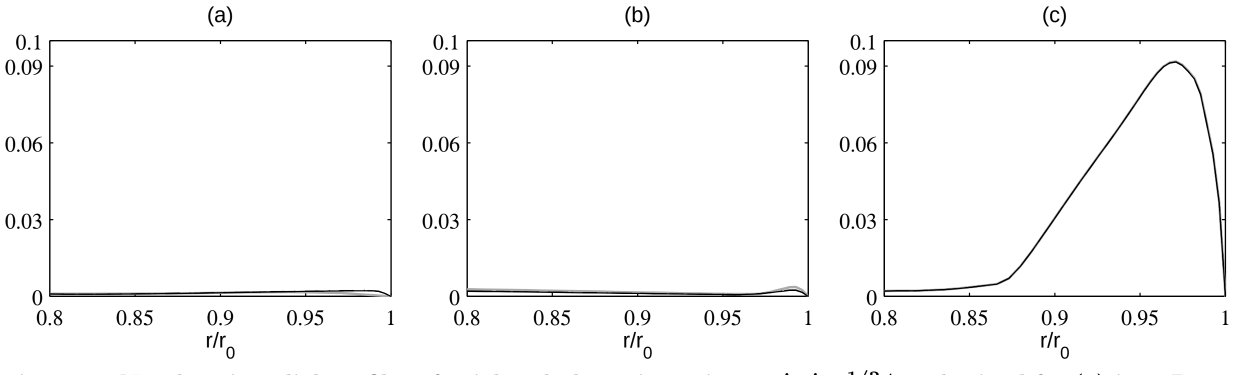

Figure 5. Nozzle-exit radial profiles of axial turbulence intensity $< u'_z u'_z >^{1/2}/u_j$ obtained for (a) jetv0D0200, (b) jetv0D0025 and (c) jetv9D0150; same line types as in figure 4 .

The profiles calculated using gridz60, gridz47 and gridz40 are superimposed, indicating that the initial conditions of the jets do not change with the grid. This is particularly true in figures 4(c) and 5(c) for jetv9D0150, whose upstream boundary layers are forced inside the nozzle to generate significant exit velocity fluctuations. Furthermore, the results agree with those from previous LES performed using coarser grids, also shown in the figures. A small difference can however be noted in figure 4(b) for the mean velocity profile of jetv0D0025, which is slightly thinner in the simulation using gridv0D0025old.

The nozzle-exit mean velocity profiles are similar to the laminar profiles imposed at the nozzle inlet, and has momentum thicknesses of $\delta_\theta = 0.0237r_0$ in jetv0D0200, $\delta_\theta = 0.0036r_0$ in jetv0D0025 and $\delta_\theta = 0.0185r_0$ in jetv9D0150. Compared to experiments,[59] the jet boundary layers are thick in the first and third case, and thin in the second case. The peak turbulence intensities u'_e/u_j are close to 0.2% in jetv0D0200 and to 0.3% in jetv0D0025, and they are equal to 9.16% in jetv9D0150. The first two jets are thus initially fully laminar, whereas the third one is initially highly disturbed. The nozzle-exit conditions in the latter jet are comparable to those measured by Zaman[24,25] in a tripped jet at $\mathrm{Re}_D = 10^5$. They are discussed in more detail in a paper[41] providing velocity spectra as a function of axial and azimuthal wavenumbers.

B. Vorticity snapshots

Snapshots of the vorticity norm calculated between $z = 0$ and $z = 30r_0$ for the three jets using gridz60, gridz47 and gridz40 are represented in figures 6(a-c), 7(a-c) and 8(a-c). For the comparison, vorticity snapshots from the previous studies using coarser grids are displayed in figures 6(d), 7(d) and 8(d). In the two jets with fully laminar upstream conditions, as expected,[27,28] roll-ups and pairings of vortical structures are observed downstream of the nozzle. The initially laminar jet with thick nozzle-exit boundary layers also develops more rapidly than the two others, leading to a potential core ending around $z = 10r_0$ in jetv0D0200, but around $z = 15r_0$ in jetv0D0025 and jetv9D0150.

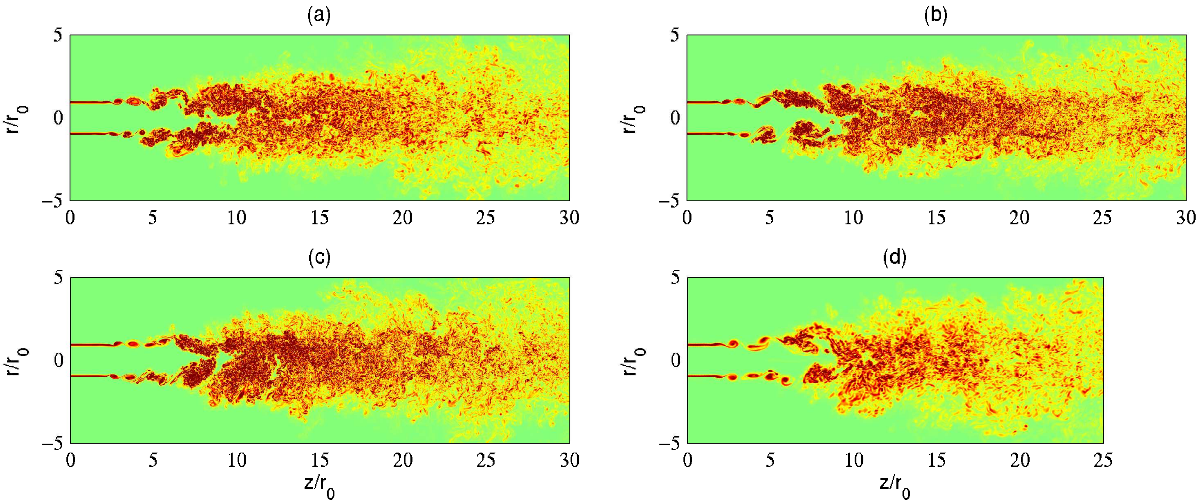

Figure 6. Representation of vorticity norm obtained for jetv0D0200 using (a) gridz60, (b) gridz47, (c) gridz40 and (d) gridv9D0150old. The color scale ranges up to the level of $6.5u_j/r_0$.

While these snapshots must be interpreted with caution, they suggest that the effects of the grid on the vorticity field are rather small for jetv0D0200, but significant for the two other jets, see for instance figures 7(c,d) and figures 8(c,d) obtained for jetv0D0025 and jetv9D0150 using gridz40 and the grids of previous studies. When a finer grid is used, the vorticity levels are found to increase, especially in the outer lateral flow regions and near the jet centerline. In addition, two flow features of importance in terms of jet development and noise generation are more clearly visible. The first one concerns the presence of large-scale structures in the turbulent mixing layers upstream of the end of the potential core, resembling the coherent structures revealed by the visualizations of Brown & Roshko,[60] and the second one is the merging of the mixing layers on the jet axis downstream of the jet core. It can be noted that both are very difficult to see in figure 7(d) using gridv0D0025old for jetv0D0025.

C. Shear-layer properties

The variations over $0 \le z \le 20r_0$ of the shear-layer momentum thickness δ_θ in the three jets are presented in figure 9. As examples, the experimental data obtained by Fleury[62] and Castelain[63] in isothermal jets at

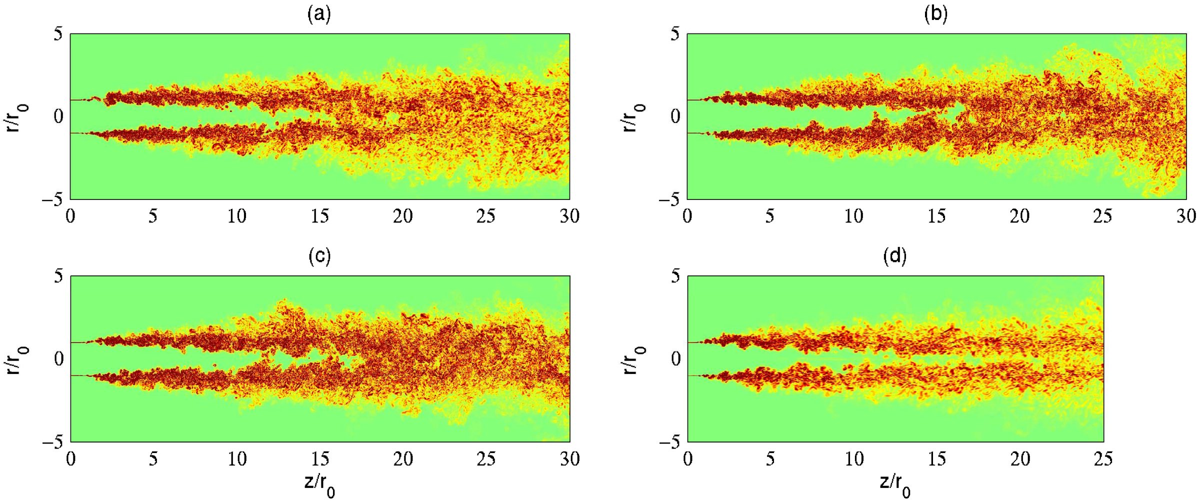

Figure 7. **Representation of vorticity norm obtained for jetv0D0025 using (a) gridz60, (b) gridz47, (c) gridz40 and (d) gridv9D0150old. The color scale ranges up to the level of $6.5u_j/r_0$.**

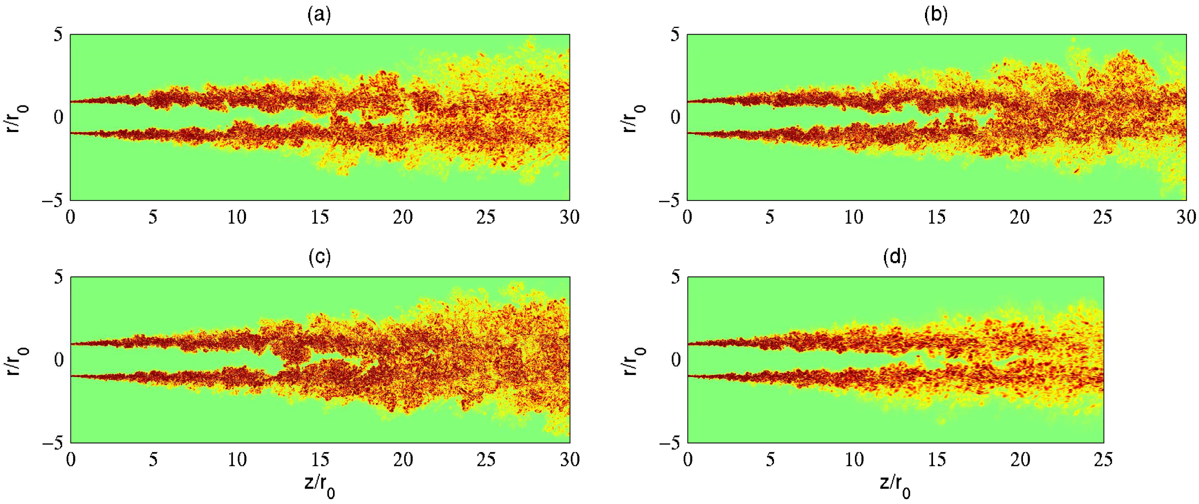

Figure 8. **Representation of vorticity norm obtained for jetv9D0150 using (a) gridz60, (b) gridz47, (c) gridz40 and (d) gridv9D0150old. The color scale ranges up to the level of $6.5u_j/r_0$.**

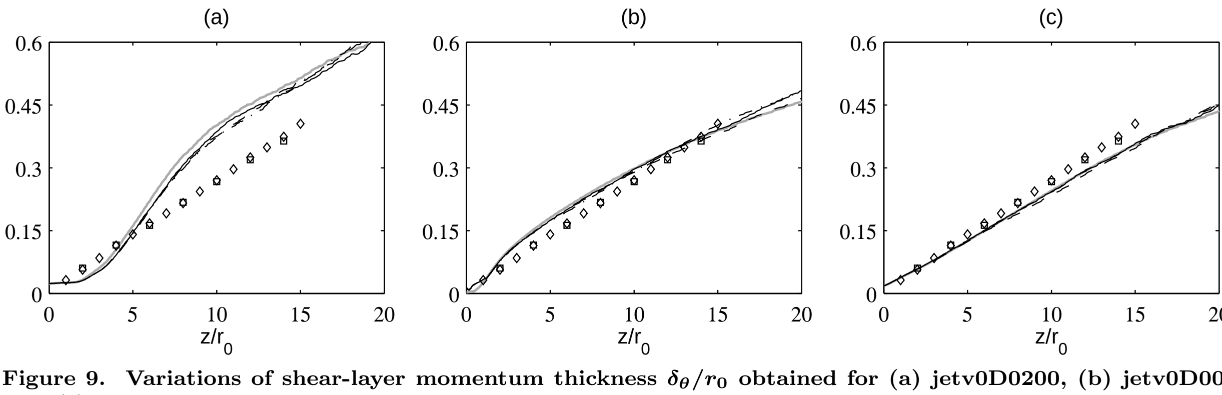

Figure 9. **Variations of shear-layer momentum thickness δ_θ/r_0 obtained for (a) jetv0D0200, (b) jetv0D0025 and (c) jetv9D0150 using ——— gridz60, – – – gridz47 and – · – gridz40; ——— results obtained using (a) gridv0D0200old, (b) gridv0D0025old and (c) gridv9D0150old; measurements for isothermal jets at $M = 0.9$ of ◇ Fleury[62] at $Re_D = 7.7 \times 10^5$, and □ Castelain[63] at $Re_D = 10^6$.**

M = 0.9 and $\mathrm{Re}_D \geq 7.7 \times 10^5$ are also shown. The shear layers develop very rapidly in the initially laminar jet with thick exit boundary layers, but at a lower rate in the two other jets, comparable to that in the experiments. Above all, for the three jets considered, the different curves obtained using the present and previous grids are very close, indicating that the shear-layer spreading does not depend appreciably on the grid resolution.

The rms values of axial and radial velocity fluctuations estimated along the nozzle-lip line at $r = r_0$ between $z = 0$ and $z = 25r_0$ are displayed in figures 10 and 11, respectively. As in the preceding figure, measurements for isothermal, Mach 0.9 jets at high Reynolds numbers are also drawn. Note that they represent peak rms values and not of rms values at $r = r_0$. The influence of the initial jet flow state on the axial evolution of the turbulence intensities is clearly visible.[28] Indeed, a well-marked peak appear downstream of the nozzle exit in jetv0D0200 and jetv0D0025, whereas a mononotic growth, followed by a region of nearly constant values, is observed in jetv9D0150. The peak in the two initially laminar jets is due to the first stage of pairing of the shear-layer coherent vortices.

Concerning the sensitivity to the grid, the rms velocity profiles obtained using gridz60, gridz47 and gridz40 are very similar for the three jets. This is particularly true in figure 11 for the radial turbulence intensity, whose value at $z = 15r_0$, for instance, increases only from 10.2% up to 10.5% in jetv0D0025, and from 10.6% up to 10.9% in jetv9D0150 when the grid is refined. Compared to the previous studies using coarser grids, the turbulence levels at large distances from the nozzle exit are higher in the present LES, especially for jetv0D0025 and jetv9D0150. For example, values of $< u'_z u'_z >^{1/2}/u_j = 15.1\%$ and 12.9% are found at $z = 15r_0$ using gridz40 and gridv0D0025old for the first jet. For the initially laminar jet with thin exit boundary layers and the initially disturbed jet, more precisely, the turbulence intensities remain high or slightly increase nearly up to $z = 20r_0$ in the present simulations, which is in line with the measurements, whereas they begin to decrease farther upstream, and apparently too early, in the previous simulations, see notably in figure 10(c).

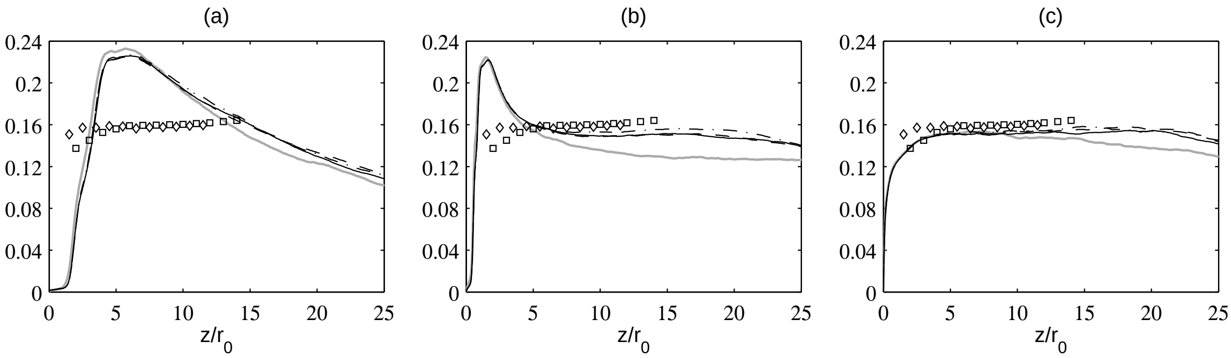

Figure 10. Variations of axial turbulence intensity $< u'_z u'_z >^{1/2}/u_j$ obtained at $r = r_0$ for (a) jetv0D0200, (b) jetv0D0025 and (c) jetv9D0150 using ——— gridz60, – – – gridz47 and – · – · gridz40; ——— results obtained using (a) gridv0D0200old, (b) gridv0D0025old and (c) gridv9D0150old; peak values measured in isothermal jets at M = 0.9 by ◇ Fleury[62] at $\mathrm{Re}_D = 7.7 \times 10^5$, and □ Castelain[63] at $\mathrm{Re}_D = 10^6$.

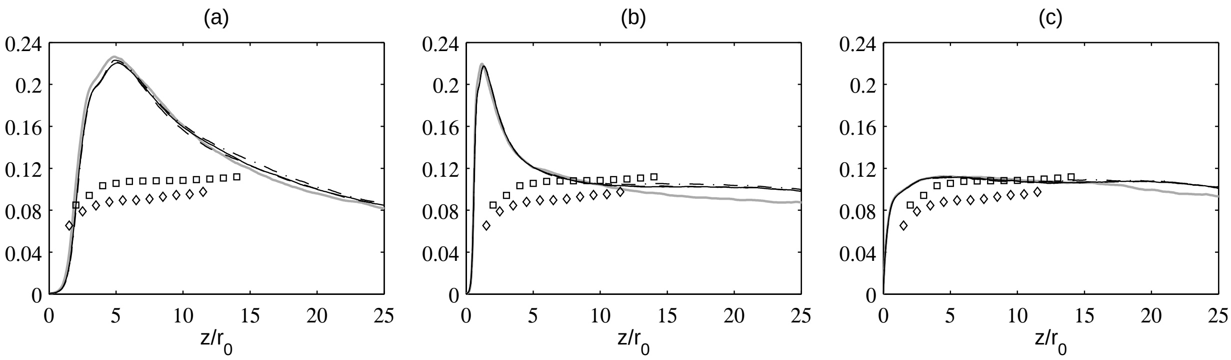

Figure 11. Variations of radial turbulence intensity $< u'_r u'_r >^{1/2}/u_j$ obtained at $r = r_0$ for (a) jetv0D0200, (b) jetv0D0025 and (c) jetv9D0150; same line and symbol types as in figure 10.

The effects of the grid on the spectral properties of velocity fluctations are investigated by considering spectra at $r = r_0$. The spectra computed at $z = 10r_0$ for jetv0D0200 and at $z = 15r_0$ for jetv0D0025 and jetv9D0150, that is near the end of the jet potential core, are presented in figure 12 as a function of the Strouhal number St_D. For all jets, they are dominated by low-frequency components at $\mathrm{St}_D \leq 0.15$. Moreover, the spectra obtained using gridz60, gridz47 and gridz40 do not differ appreciably. For jetv9D0150, in figure 12(c), they show higher levels at low frequencies, and inversely lower levels over $0.6 \leq \mathrm{St}_D \leq 3$, than the spectra from the LES using gridv9D0150old. The use of finer grids thus leads to stronger large-scale structures and weaker fine-scale structures. This result is consistent with the observation made on the vorticity fields of figures 7 and 8, namely that coherent structures can be more easily seen in the turbulent mixing layers in the present LES than in the previous ones.

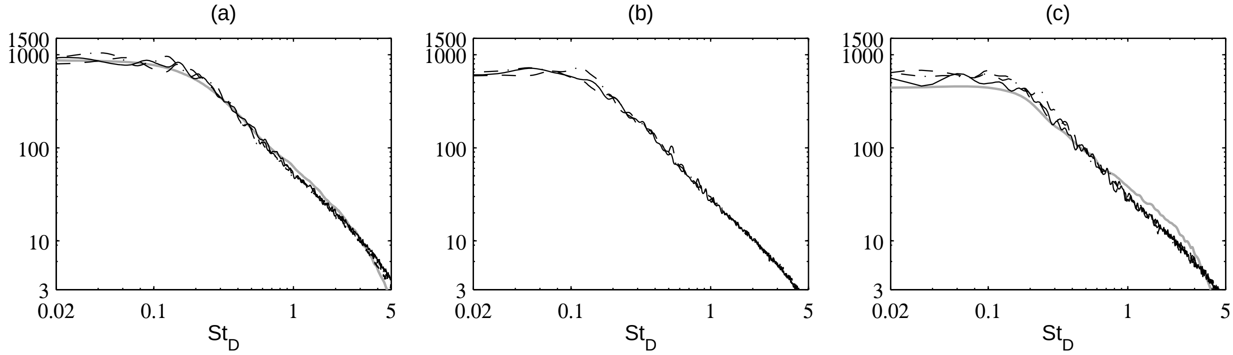

Figure 12. Power spectral densities of axial velocity fluctuations u_z', multiplied with $10^4/u_j^2$, obtained at $r = r_0$ for (a) jetv0D0200 at $z = 10r_0$, and for (b) jetv0D0025 and (c) jetv9D0150 at $z = 15r_0$, using ——— gridz60, — — — gridz47 and — · — · gridz40, as a function of St_D; ——— results obtained using (a) gridv0D0200old and (c) gridv9D0150old.

D. Centerline flow properties

The variations of the centerline mean axial velocity in the three jets are presented in figure 13. Experimental data for isothermal jets at $\mathrm{M} = 0.9$ at $\mathrm{Re}_D \geq 7.7 \times 10^5$ are also depicted for the comparison. As noted in previous section, the jet flow development is more rapid in jetv0D0200 than in jetv0D0025 and jetv9D0150. This leads to a potential core ending at about $z_c = 9.2r_0$ in the first jet, but at about $z_c = 15.4r_0$ and $z_c = 16r_0$ in the two others, with z_c being defined as the axial distance at which the centerline mean velocity is equal to $0.95u_j$. In all cases, the velocity profiles from the LES using gridz60, gridz47 and gridz40are very close to each others. For jetv0D0200, they are similar to the profile obtained using gridv0D0200old. For jetv9D0150, in the same way, they are nearly superimposed on the profile obtained using gridv9D0150old up to $z = 20r_0$, and then they are slightly below. For jetv0D0025, on the contrary, significant differences are

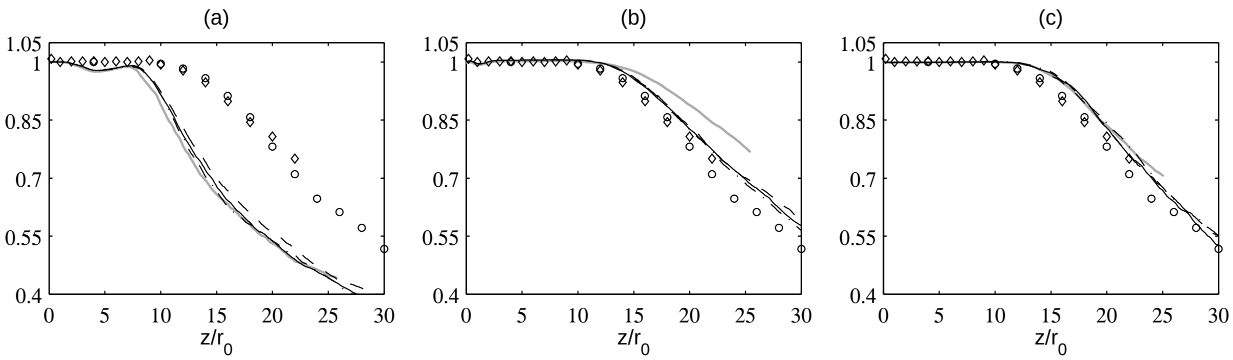

Figure 13. Variations of mean axial velocity $< u_z > /u_j$ obtained at $r = 0$ for (a) jetv0D0200, (b) jetv0D0025 and (c) jetv9D0150 using ——— gridz60, — — — gridz47 and — · — · gridz40; ——— results obtained using (a) gridv0D0200old, (b) gridv0D0025old and (c) gridv9D0150old; measurements for isothermal jets at $\mathrm{M} = 0.9$ of ○ Lau *et al.*[64] at $\mathrm{Re}_D = 10^6$, and ◇ Fleury *et al.*[61] at $\mathrm{Re}_D = 7.7 \times 10^5$.

found with respect to the result of the previous simulation using a coarser grid. In the present LES, the jet potential core is shorter, with $z_c = 15.2r_0$ using gridz60 vs. $z_c = 16.8r_0$ using gridv0D0025, and the velocity decay farther downstream is faster These discrepancies can be related to the poor mixing of the shear-layer turbulent structures that seems to happen on the jet axis in figure 7(d).

The variations of the axial and radial turbulence intensities along the jet centerline between $z = 0$ and $z = 30r_0$ are plotted in figures 14 and 15, together with measurements for isothermal, high Reynolds number jets at $\mathrm{M} = 0.9$. Despite the fact that they may not be well converged in time because of the impossibility of averaging in the azimuthal direction, especially for jetv9D0150 simulated over a time period of $300r_0/u_j$, the profiles obtained using gridz60, gridz47 and gridz40 are fairly comparable. They are even in good agreement in figure 15 for the radial velocity component. They reach peak values at $z \simeq 12r_0$ in jetv0D0200 and at $z \simeq 23r_0$ in jetv0D0025 and jetv9D0150, which are close to about 15%, 13% and 13.5% for u'_z, and about 13.5%, 10% and 10.5% for u'_r in the three jets, respectively. For jetv0D0200, the results are similar to those from the LES with gridv0D0200old. For the two other jets, the centerline turbulence intensities are higher in the present simulations than in the previous ones. In particular, the peak values in jetv0D0025 and jetv9D0150 are only 11.4% and 11.4% for u'_z, and 5.6% and 9.4% for u'_r in the latter simulations. The very low levels of radial velocity fluctuations in the LES of jetv0D0025 using gridv0D0025old are most likely due to the lack of turbulent structures on the centerline revealed in figure 7(d). One reason for that may be the effective number of points of only $n_\theta^{axis} = 8$ in the azimuthal direction close to the jet axis in this case, reported in table 2.

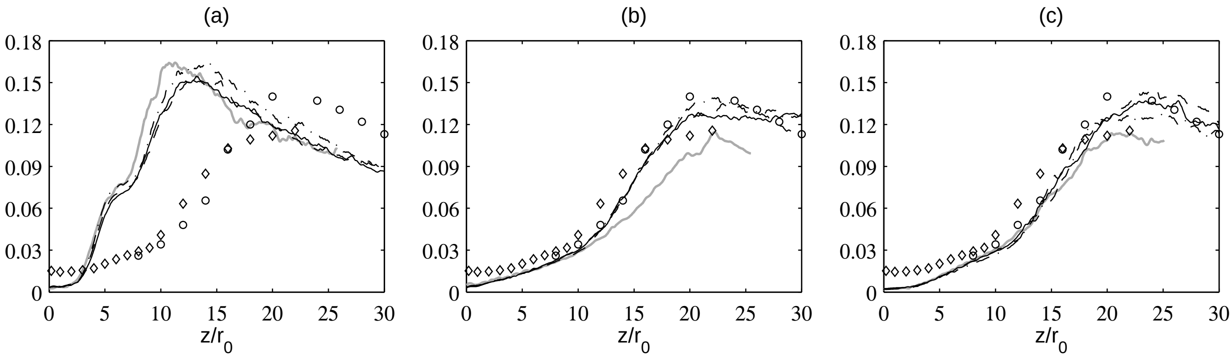

Figure 14. Variations of axial turbulence intensity $< u'_z u'_z >^{1/2}/u_j$ obtained at $r = 0$ for (a) jetv0D0200, (b) jetv0D0025 and (c) jetv9D0150; same line and symbol types as in figure 13.

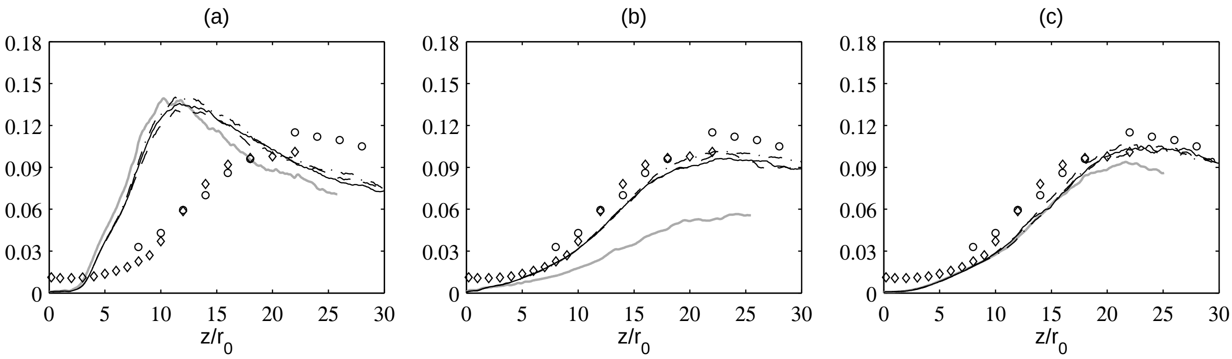

Figure 15. Variations of radial turbulence intensity $< u'_r u'_r >^{1/2}/u_j$ obtained at $r = 0$ for (a) jetv0D0200, (b) jetv0D0025 and (c) jetv9D0150; same line and symbol types as in figure 13.

Finally, the spectra of axial velocity fluctuations calculated on the jet axis at $z = 15r_0$ for jetv0D0200 and at $z = 25r_0$ for jetv0D0025 and jetv9D0150, that is just downstream of the turbulence intensity peaks, are presented in figure 16 as a function of St_D. As pointed out above, they may not be very well converged, especially for jetv9D0150 for with the simulation time only contains 15 periods associated with $\mathrm{St}_D = 0.1$. Despite this issue, maybe causing the discrepancies observed for $\mathrm{St}_D < 0.1$ in figure 16(c), the spectra obtained using the present grids are very much alike. Compared to the spectra from the previous simulations, they are very similar for jetv0D0200, but show higher low-frequency levels for the two other jets. As is the case along the nozzle-lip line, see in figure 12(c) and the discussion of the end of section III.C, stronger large-scale structures are thus present on the jet centerline in the present LES. This suggests that the use of fine grids is necessary to properly form the larger flow structures, sometimes also called coherent structures, in the last two jets of this study.

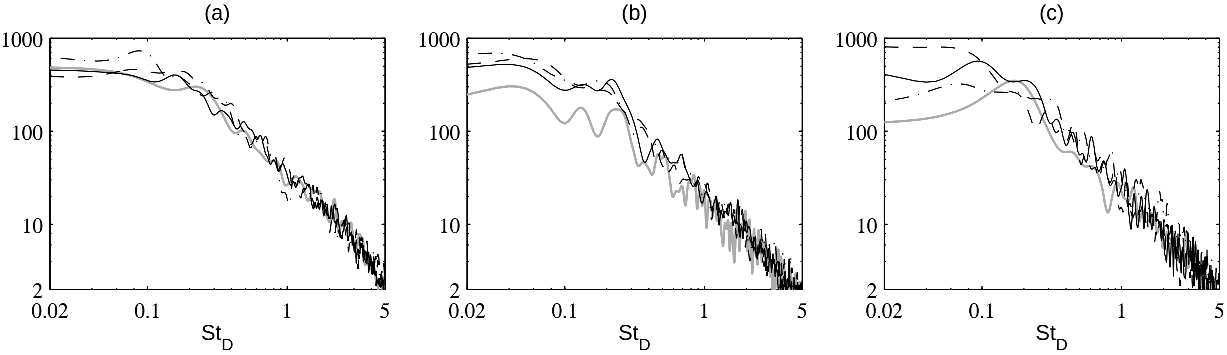

Figure 16. Power spectral densities of axial velocity fluctuations u'_z, multiplied with $10^4/u_j^2$, obtained at $r = 0$ for (a) jetv0D0200 at $z = 15r_0$, and for (b) jetv0D0025 and (c) jetv9D0150 at $z = 25r_0$, using ——— gridz60, — — — gridz47 and — · — · gridz40, as a function of St_D; ——— results obtained using (a) gridv0D0200old, (b) gridv0D0025old and (c) gridv9D0150old.

IV. Jet acoustic fields

A. Pressure snapshots

Snapshots of the vorticity norm and of the fluctuating pressure obtained for the three jets in the LES using gridz60 with physical extents of $L_r = 20r_0$ and $L_z = 60r_0$ in the radial and axial directions are represented in figure 17 for $r \leq 4r_0$ and $r \geq 4r_0$, respectively. In agreement with previous studies,[27,30] the acoustic levels are higher for the two initially fully laminar jets. In these jets, strong circular acoustic waves are generated by vortex pairings early on in the mixing layers, which is not the case in the initially disturbed jet. Their associated wavelengths are shorter in jetv0D0025 than in jetv0D0200 due to the thinner nozzle-exit boundary layers in the former case. Farther downstream, large-scale near-field pressure fluctuations, classically attributed to the flow coherent structures,[58] are observed in the close vicinity of the jets. Very low-frequency waves propagating in the downstream direction are also found in all cases, see in figure 17(c) for the jet which does not radiate vortex-pairing noise.

In order to illustrate the far field obtained for jetv9D0150 with highly disturbed initial flow conditions, a snapshot of the vorticity issued from the LES of that jet using gridz60 and of the pressure computed by solving the isentropic linearized Euler equations from the LES data at $z = -1.5r_0$, $r = L_r = 20r_0$ and $z = L_z = 60r_0$, as reported in section II.E, is displayed in figures 3. The two main features of subsonic jet noise[14,37–39] appear clearly. The first one is the pronounced directivity in the downstream direction with a peak angle around $\varphi = 30^\mathrm{o}$ relative to the jet axis. The second one is the change in spectral content with the radiation angle. In particular, very low-frequency components characterized by wavelengths $\lambda \simeq 15r_0$, yielding Strouhal numbers $\mathrm{St}_D \simeq 0.15$, are dominant for shallow angles, which does not seem to be the case for wide angles.

B. Near-field acoustic spectra

The pressure spectra computed from the LES data at $r = 15r_0$ from the jet axis at $z = 0$, $z = 20r_0$ and $z = 40r_0$ are presented as a function of St_D in figures 18, 19 and 20. Three axial positions are considered in order to get a complete picture of the near acoustic fields of the jets. By way of illustration, the measurements available in Bogey *et al.* [37] for an isothermal jet at $\mathrm{M} = 0.9$ and $\mathrm{Re}_D = 7.9 \times 10^5$ are also plotted in the figures. As expected,[37] the shape of the spectra varies significantly with the axial distance. They are broadband at $z = 0$ and $z = 20r_0$, but they are clearly dominated by a low-frequency peak at $z = 40r_0$. Additional noise components are noted in the spectra of the two initially laminar jets compared to the

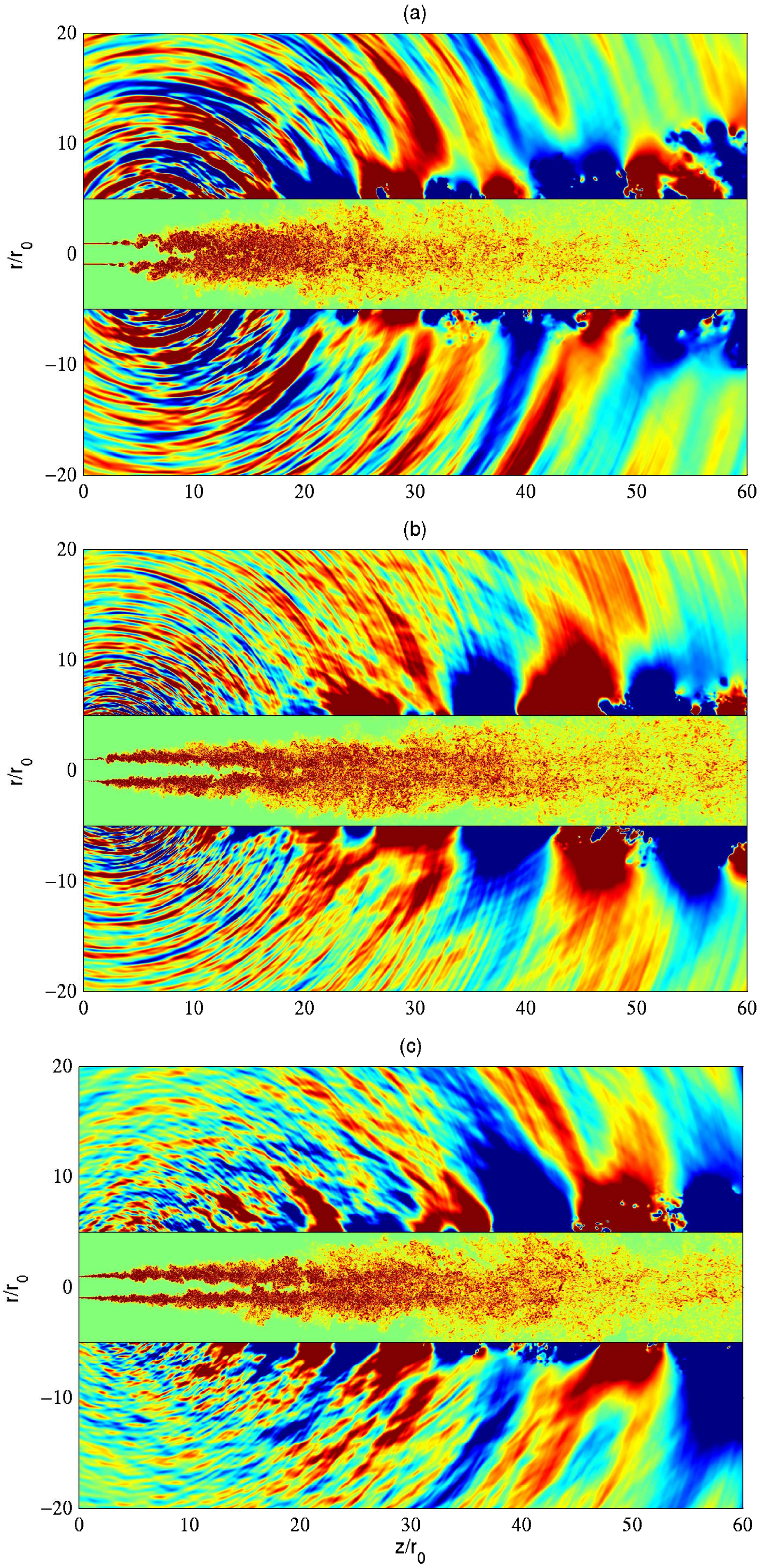

Figure 17. Representation of vorticity norm inside the jet flow and of pressure fluctuations outside, obtained for (a) jetv0D0200, (b) jetv0D0025 and (c) jetv9D0150 using gridz60. The color scales range up to the level of $4u_j/r_0$ for vorticity, and (a) from -90 to 90 Pa, (b) from -60 to 60 Pa, and (c) from -40 to 40 Pa for pressure.

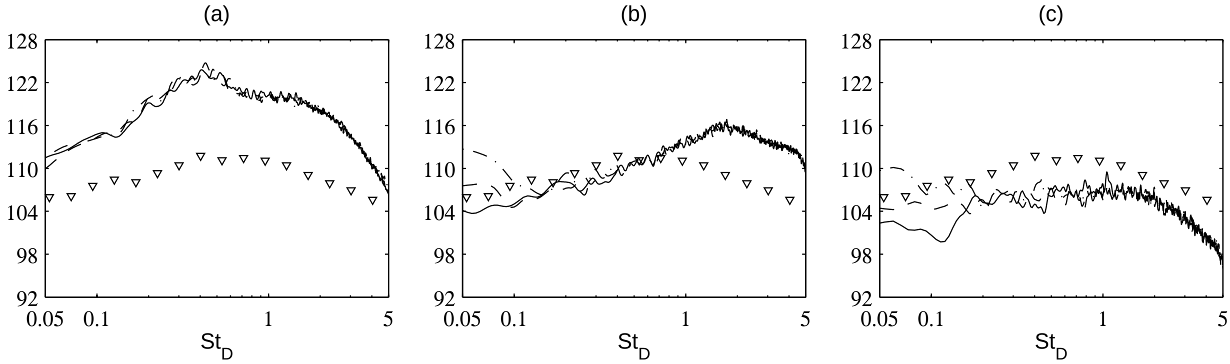

Figure 18. Sound pressure levels obtained at $r = 15r_0$ and $z = 0$ for (a) jetv0D0200, (b) jetv0D0025 and (c) jetv9D0150 using ——— gridz60, − − − gridz47 and − · − · gridz40, as a function of St_D, in dB/St_D; ▽ measurements of Bogey *et al.*[37] for an isothermal jet at M = 0.9 and $\mathrm{Re}_D = 7.9 \times 10^5$.

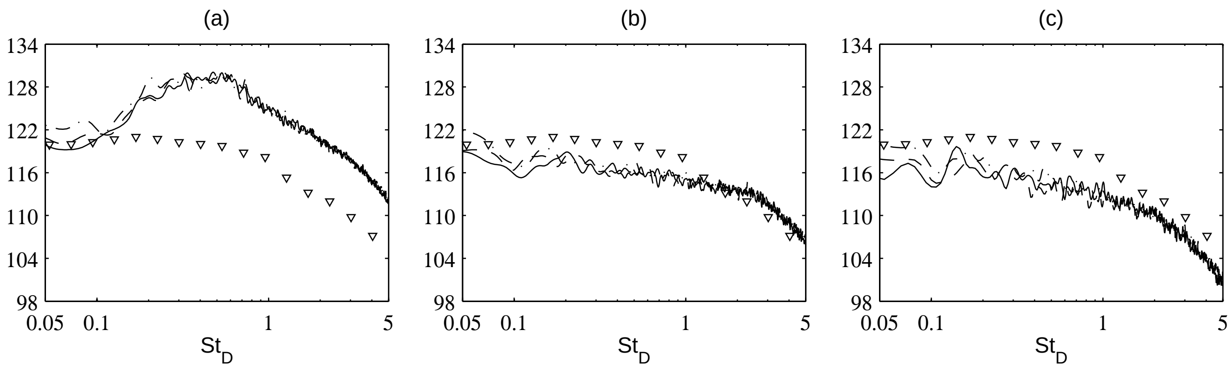

Figure 19. Sound pressure levels obtained at $r = 15r_0$ and $z = 20r_0$ for (a) jetv0D0200, (b) jetv0D0025 and (c) jetv9D0150 , as a function of St_D, in dB/St_D; same line and symbol types as in figure 18.

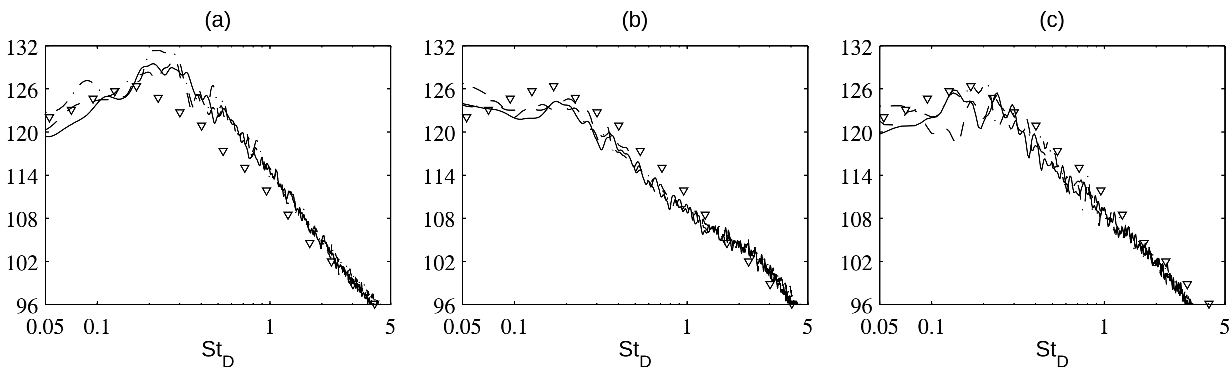

Figure 20. Sound pressure levels obtained at $r = 15r_0$ and $z = 40r_0$ for (a) jetv0D0200, (b) jetv0D0025 and (c) jetv9D0150, as a function of St_D, in dB/St_D; same line and symbol types as in figure 18.

initially highly disturbed jet. They are well visible at $z = 0$ in figure 18, and also apparent at $z = 20r_0$ in figure 19. At the latter position, they are centered around a Strouhal number of $\mathrm{St}_D = 0.5$ in jetv00D0200 and of $\mathrm{St}_D = 2.2$ in jetv0D0025, which correspond to the vortex-pairing frequencies evaluated from velocity spectra in the mixing layers. Finally, and most importantly, for the three jets and at the three positions, the spectra obtained in the LES using gridz60, gridz47 and gridz40 are nearly superimposed for $\mathrm{St}_D \geq 0.1$. For lower frequencies, the acoustic levels are higher in the simulations of jetv0D0025 and jetv9D0150 using gridz47 and, even more, gridz40, at $z = 0$ and $z = 20r_0$. This extra noise could be due to the generation of spurious waves at the outflow boundary of the LES.

C. Far-field acoustic spectra

The pressure spectra calculated at a distance of $150r_0$ of the nozzle exit for the angles $\varphi = 40^o$ and $\varphi = 90^o$ relative to the jet direction, by solving the ILEE from the LES near-field data, are shown in figures 21 and 22. They are compared with the results of previous simulations using coarser grids, and with the experimental data acquired by Bridges & Brown[17] at the same distance for an isothermal jet at $M = 0.9$ and $\mathrm{Re}_D = 10^6$. As pointed out for the near-field spectra, the initially fully laminar jets radiate strong additional noise components. In the spectra at $\varphi = 90^o$ of figure 22, these components are centered around the vortex-pairing Strouhal numbers, namely $\mathrm{St}_D = 0.5$ in jetv0D0200 and $\mathrm{St}_D = 2.2$ in jetv0D0025.

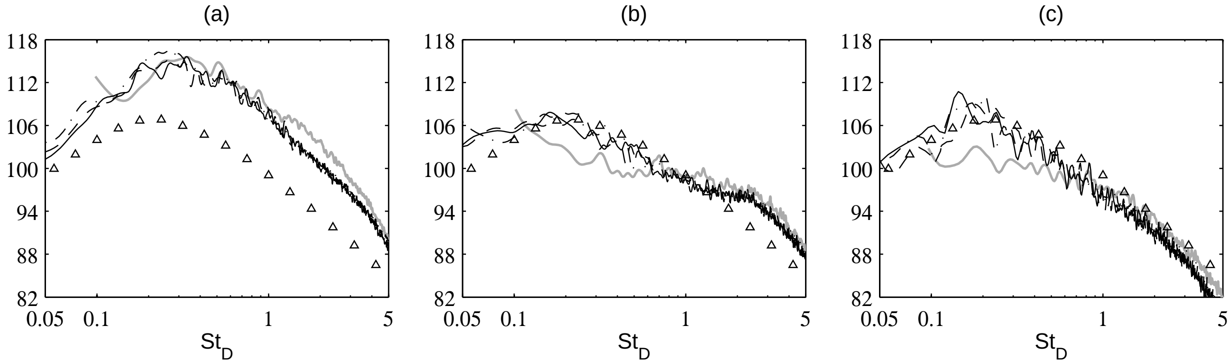

Figure 21. Sound pressure levels obtained at $150r_0$ from the nozzle exit and $\varphi = 40^o$ relative to the jet direction for (a) jetv0D0200, (b) jetv0D0025 and (c) jetv9D0150 using ——— gridz60, − − − gridz47 and − · − · gridz40, as a function of St_D, in dB/St_D; ——— results obtained using (a) gridv0D0200old, (b) gridv0D0025old and (c) gridv9D0150old; △ measurements of Bridges & Brown[17] for an isothermal jet at $M = 0.9$ and $\mathrm{Re}_D = 10^6$.

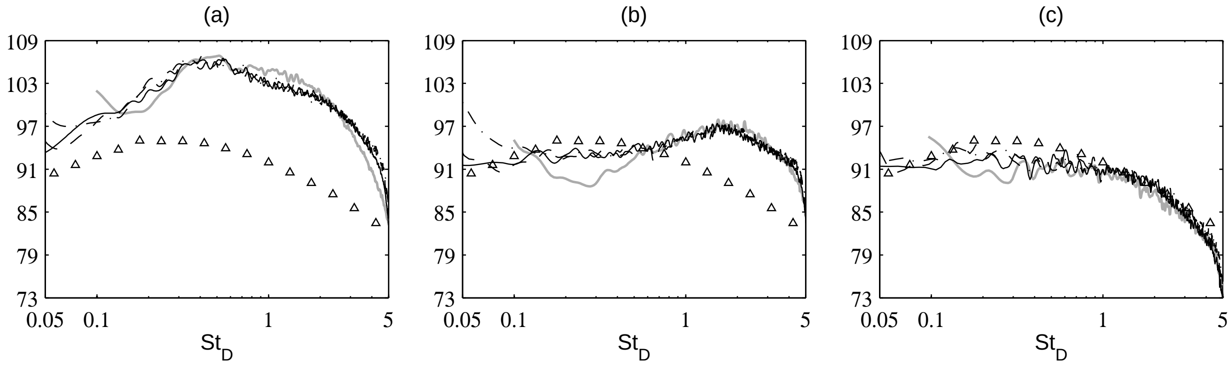

Figure 22. Sound pressure levels obtained at $150r_0$ from the nozzle exit and $\varphi = 90^o$ relative to the jet direction for (a) jetv0D0200, (b) jetv0D0025 and (c) jetv9D0150, as a function of St_D, in dB/St_D; same line and symbol types as in figure 21.

More remarkably, the spectra obtained from the simulations using gridz60, gridz47 and gridz40 are very similar in all cases, except for $\mathrm{St} \leq 0.1$ in figure 22(b) maybe due to reflections at the LES outflow boundary as mentioned above. For jetv0D0200, they do not differ much from the spectra from the previous study using gridv0D0200old For jetv0D0025 and jetv9D0150, they are comparable with the results of previous studies using coarser grids for St ≥ 0.5, but they exhibit higher levels for St ≤ 0.5. The increase in grid resolution, which results in higher turbulence intensities and stronger large-scale structures just upstream and downstream of the end of the potential core, as shown in sections III.C and III.D, thus also leads to more low-frequency noise. Compared to the experimental data, the spectra obtained in the present LES for jetv0D0150 are in good agreement at $\varphi = 40^o$ over the whole frequency range in figure 21(c), and at $\varphi = 90^o$ for $\mathrm{St}_D \geq 0.8$ in figure 22(c). At the latter angle, for $\mathrm{St}_D \leq 0.8$, the sound levels predicted by the LES are approximately 2.5 dB below the measurements. For jetv00D0025, in figure 22(b), the difference is smaller, and is about 1 dB. A similar discrepancy with respect to experiments at $\mathrm{Re}_D \simeq 10^6$ was observed by Uzun & Hussaini[65] for cold jets at M = 0.9 and $\mathrm{Re}_D = 10^5$ computed using 370 million points. It could be caused by the mismatch of the nozzle-exit flow conditions and Reynolds number between the simulations and experiments.

V. Conclusion

Three isothermal round jets at a Mach number of 0.9 and a Reynolds number of 10^5 with controlled nozzle-exit conditions, namely two initially fully laminar jets and an initially highly disturbed jet, were simulated using three fine cylindrical grids with increasing resolution. The properties of the flow, near and far acoustic fields of the jets were described, and found to be very similar for the different grids.

Compared to the results from previous studies using coarser grids, the present results were found to be comparable for the initially laminar jet with thick nozzle-exit boundary layers, but significantly different for the the initially laminar jet with thin boundary layers and for the initially disturbed jet. In the two latter cases, the use of a finer grid resolution in the axial direction for $z \geq 5r_0$, and in the radial direction in the outer region of the shear layers led to a more rapid jet development and to higher turbulence intensities just upstream and downstream of the jet potential core. More surprisingly, this also resulted in the presence of stronger large-scale structures, and in the generation of more low-frequency noise.

The present study thus highlights the importance of the largest turbulent scales, also referred to as coherent structures, in free shear flows, and their crucial role in terms of flow development and sound production. Therefore, these structures must be properly taken into account in numerical simulations. This should be done by using mesh spacings small enough that they are well discretized, which is generally relatively easy, but also that they can form, which may be more difficult. In some cases, indeed, including the last two subsonic jets considered in this study, this seems to require the computation of a wide range of fine-scale structures.

Acknowledgments

This work was granted access to the HPC resources of FLMSN (Fédération Lyonnaise de Modélisation et Sciences Numériques), partner of EQUIPEX EQUIP@MESO, and of the resources of IDRIS (Institut du Développement et des Ressources en Informatique Scientifique) under the allocation 2015-2a0204 made by GENCI (Grand Equipement National de Calcul Intensif). It was performed within the framework of the Labex CeLyA of Université de Lyon, operated by the French National Research Agency (Grant No. ANR-10-LABX-0060/ANR-11-IDEX-0007).

References

[1]Tam, C.K.W., "Computational Aeroacoustics: Issues and Methods," *AIAA J.*, Vol. 33, No. 10, 1995, pp. 1788-1796.

[2]Colonius, T. and Lele, S.K., "Computational aeroacoustics: progress on nonlinear problems of sound generation," *Progress in Aerospace Sciences*, Vol. 40, 2004, pp. 345-416.

[3]Bailly, C. and Bogey, C., "Contributions of CAA to jet noise research and prediction," *Int. J. Comput. Fluid Dyn.*, Vol. 18, No. 6, 2004, pp. 481-491.

[4]Wang, M., Freund, J.B., and Lele, S.K., "Computational prediction of flow-generated sound," *Annu. Rev. Fluid. Mech.*, Vol. 38, 2006, pp. 483-512.

[5]Bodony, D.J. and Lele, S.K., "On the current status of jet noise predictions using large-eddy simulation," *AIAA J.*, Vol. 46, No. 2, 2008, pp. 364-380.

[6]Shur, M.L., Spalart, P.R. and Strelets, M.Kh., "LES-based evaluation of a microjet noise reduction concept in static and flight conditions," *J. Sound Vib.*, Vol. 330, No. 17, 2011, pp. 4083-4097.

[7]Fosso Pouangué, A., Sanjosé, M., Moreau, S., Daviller, G., and Deniau, H., "Subsonic jet noise simulations using both structured and unstructured grids," *AIAA J.*, Vol. 53, No. 1, 2015, pp. 55-69.

[8]Bogey, C. and Marsden, O., "Simulations of two initially highly disturbed jets with experiment-like nozzle-exit boundary-layer properties," to appear in *AIAA J.*, 2016. See also AIAA Paper 2015-0510, 2015.

[9]Brès, G.A., Jaunet, V., Le Rallic, M., Jordan, P., Colonius, T., and Lele, S.K., "Large eddy simulation for jet noise: the importance of getting the boundary layer right," AIAA Paper 2015-2535, 2015.

[10]Le Bras, S., Deniau, H., Bogey, C., and Daviller, G., "Development of compressible large-eddy simulations combining high-order schemes and wall modeling," AIAA Paper 2015-3135, 2015.

[11]Bogey, C., Bailly, C., and Juvé, D., "Noise investigation of a high subsonic, moderate Reynolds number jet using a compressible LES," *Theoret. Comput. Fluid Dynamics*, Vol. 16, No. 4, 2003, pp. 273-297.

[12]Panda, J., Seasholtz, R.G., and Elam, K.A., "Investigation of noise sources in high-speed jets via correlation measurements," *J. Fluid Mech.*, Vol. 537, 2005, pp. 349-385.

[13]Bogey, C. and Bailly, C., "An analysis of the correlations between the turbulent flow and the sound pressure field of subsonic jets," *J. Fluid Mech.*, Vol. 583, 2007, pp. 71-97.

[14]Tam, C.K.W., Viswanathan, K., Ahuja, K.K., and Panda, J., "The sources of jet noise: experimental evidence," *J. Fluid Mech.*, Vol. 615, 2008, p. 253-292.

[15]Bridges, J. and Wernet, M.P., "Validating large-eddy simulation for jet aeroacoustics," *J. Propul. Power*, Vol. 28, No. 2, 2012, pp. 226-234.

[16]Viswanathan, K., "Jet aeroacoustic testing: issues and implications," *AIAA J.*, Vol. 41, No. 9, 2003, pp. 1674-1689.

[17]Bridges, J. and Brown, C.A., "Validation of the small hot jet acoustic rig for aeroacoustics," AIAA Paper 2005-2846, 2005. See also: Brown, C. and Bridges, J., "Small hot jet acoustic rig validation," NASA TM-2006-214234, 2006.

[18]Bridges, J. and Wernet, M.P., "Establishing consensus turbulence statistics for hot subsonic jets," AIAA 2010-3751, 2010.

[19]Viswanathan, K., "Aeroacoustics of hot jets," *J. Fluid Mech.*, Vol. 516, 2004, pp. 39-82.

[20]Harper-Bourne, M., "Jet noise measurements: past and present," *Int. J. Aeroacoust.*, Vol. 9, No. 4 & 5, 2010, pp. 559-588.

[21]Freund, J.B., "Noise sources in a low-Reynolds-number turbulent jet at Mach 0.9," *J. Fluid Mech.*, Vol. 438, 2001, pp. 277-305.

[22]Sandberg, R.D., Sandham, N.D., and Suponitsky, V., "DNS of compressible pipe flow exiting into a coflow," *Int. J. Heat and Fluid Flow*, Vol. 35, 2012, pp. 33-44.

[23]Bühler, S., Kleiser, L., and Bogey, C., "Simulation of subsonic turbulent nozzle-jet flow and its near-field sound," *AIAA J.*, Vol. 52, No. 8, 2014, pp. 1653-1669.

[24]Zaman, K.B.M.Q., "Effect of initial condition on subsonic jet noise," *AIAA J.*, Vol. 23, 1985, pp. 1370-1373.

[25]Zaman, K.B.M.Q., "Far-field noise of a subsonic jet under controlled excitation," *J. Fluid Mech.*, Vol. 152, 1985, pp. 83-111.

[26]Bridges, J.E. and Hussain, A.K.M.F., "Roles of initial conditions and vortex pairing in jet noise," *J. Sound Vib.*, Vol. 117, No. 2, 1987, pp. 289-311.

[27]Bogey, C. and Bailly, C., "Influence of nozzle-exit boundary-layer conditions on the flow and acoustic fields of initially laminar jets," *J. Fluid Mech.*, Vol. 663, 2010, pp. 507-539.

[28]Bogey, C., Marsden, O., and Bailly, C., "Influence of initial turbulence level on the flow and sound fields of a subsonic jet at a diameter-based Reynolds number of 10^5," *J. Fluid Mech.*, Vol. 701, 2012, pp. 352-385.

[29]Shur, M.L., Spalart, P.R. and Strelets, M.Kh., "Noise prediction for increasingly complex jets. Part I: Methods and tests," *Int. J. Aeroacoust.*, Vol. 4, No. 3&4, 2005, pp. 213-246.

[30]Bogey, C., Marsden, O., and Bailly, C., "Large-Eddy Simulation of the flow and acoustic fields of a Reynolds number 10^5 subsonic jet with tripped exit boundary layers," *Phys. Fluids*, Vol. 23, No. 3, 2011, 035104.

[31]Grosche, F.-R., "Distributions of sound source intensities in subsonic and supersonic jets," AGARD-CP-131, 1974, pp. 4-1 to 4-10.

[32]Chu, W.T. and Kaplan, R.E., "Use of a spherical concave reflector for jet-noise-source distribution diagnosis," *J. Acoust. Soc. Am.*, Vol. 59, No. 6, 1976, pp. 1268-1277.

[33]Fisher, M.J., Harper-Bourne, M., and Glegg, S.A.L., "Jet engine noise source location: The polar correlation technique," *J. Sound Vib.*, Vol. 51, No. 1, 1977, pp. 23-54.

[34]Ahuja, K.K., Massey, K.C., and D'Agostino, M.S., "A simple technique of locating noise sources of a jet under simulated forward motion," AIAA Paper 98-2359, 1998.

[35]Narayanan, S., Barber, T.J. and Polak, D.R., "High subsonic jet experiments: Turbulence and noise generation studies," *AIAA J.*, Vol. 40, No. 3, 2002, pp. 430-437.

[36]Lee, S.S. and Bridges, J., "Phased-array measurements of single flow hot jets," NASA/TM 2005-213826, 2005. See also AIAA Paper 2005-2842.

[37]Bogey, C., Barré, S., Fleury, V., Bailly, C., and Juvé, D., "Experimental study of the spectral properties of near-field and far-field jet noise," *Int. J. Aeroacoust.*, Vol. 6, No. 2, 2007, pp. 73-92.

[38]Mollo-Christensen, E., Kolpin, M.A., and Martucelli, J.R., "Experiments on jet flows and jet noise far-field spectra and directivity patterns," *J. Fluid Mech.*, Vol. 18, No. 2, 1964, pp. 285-301.

[39]Zaman, K.B.M.Q. and Yu, J.C., "Power spectral density of subsonic jet noise," *J. Sound Vib.*, Vol. 98, No. 4, 1985, pp. 519-537.

[40]Crow, S.C. and Champagne, F.H., "Orderly structure in jet turbulence," *J. Fluid Mech.*, Vol. 48, 1971, pp. 547-591.

[41]Bogey, C., Marsden, O., and Bailly, C., "On the spectra of nozzle-exit velocity disturbances in initially nominally turbulent jets," *Phys. Fluids*, Vol. 23, No. 9, 2011, 091702.

[42]Bogey, C., Marsden, O., and Bailly, C., "Effects of moderate Reynolds numbers on subsonic round jets with highly disturbed nozzle-exit boundary layers," *Phys. Fluids*, Vol. 24, No. 10, 2012, 105107.

[43]Bogey, C. and Marsden, O., "Identification of the effects of the nozzle-exit boundary-layer thickness and its corresponding Reynolds number in initially highly disturbed subsonic jets," *Phys. Fluids*, Vol. 25, No. 5, 2013, 055106.

[44]Mohseni, K. and Colonius, T., "Numerical treatment of polar coordinate singularities," *J. Comput. Phys.*, Vol. 157, No. 2, 2000, pp. 787-795.

[45]Bogey, C., de Cacqueray, N., and Bailly, C., "Finite differences for coarse azimuthal discretization and for reduction of effective resolution near origin of cylindrical flow equations," *J. Comput. Phys.*, Vol. 230, No. 4, 2011, pp. 1134-1146.

[46]Bogey, C. and Bailly, C., "A family of low dispersive and low dissipative explicit schemes for flow and noise computations," *J. Comput. Phys.*, Vol. 194, No. 1, 2004, pp. 194-214.

[47]Bogey, C., de Cacqueray, N., and Bailly, C., "A shock-capturing methodology based on adaptative spatial filtering for high-order non-linear computations," *J. Comput. Phys.*, Vol. 228, No. 5, 2009, pp. 1447-1465.

[48]Berland, J., Bogey, C., Marsden, O., and Bailly, C., "High-order, low dispersive and low dissipative explicit schemes for multi-scale and boundary problems," *J. Comput. Phys.*, Vol. 224, No. 2, 2007, pp. 637-662.

[49]Tam, C.K.W and Dong, Z., "Radiation and outflow boundary conditions for direct computation of acoustic and flow disturbances in a nonuniform mean flow., *J. Comput. Acoust.*, Vol. 4, No. 2,, 1996, pp. 175-201.

[50]Bogey, C. and Bailly, C., "Three-dimensional non reflective boundary conditions for acoustic simulations: far-field formulation and validation test cases," *Acta Acustica*, Vol. 88, No. 4, 2002, pp. 463-471.

[51]Bogey, C. and Bailly, C., "Large Eddy Simulations of transitional round jets: influence of the Reynolds number on flow development and energy dissipation," *Phys. Fluids*, Vol. 18, No. 6, 2006, 065101.

[52]Bogey, C. and Bailly, C., "Turbulence and energy budget in a self-preserving round jet: direct evaluation using large-eddy simulation," *J. Fluid Mech.*, Vol. 627, 2009, pp. 129-160.

[53]Fauconnier, D., Bogey, C., and Dick, E., "On the performance of relaxation filtering for large-eddy simulation," *J. Turbulence*, Vol. 14, No. 1, 2013, pp. 22-49.

[54]Kremer, F. and Bogey, C., "Large-eddy simulation of turbulent channel flow using relaxation filtering: resolution requirement and Reynolds number effects," *Comput. Fluids*, **116**, 17-28.

[55]Bogey, C., Barré, S., Juvé, D., and Bailly, C., "Simulation of a hot coaxial jet : direct noise prediction and flow-acoustics correlations," *Phys. Fluids*, Vol. 21, No. 3, 2009, 035105.

[56]Ahuja, K.K., Tester, B.J., and Tanna, H.K., "Calculation of far field jet noise spectra from near field measurements with true source location," *J. Sound Vib.*, Vol. 116, No. 3, 1987, pp. 415-426.

[57]Viswanathan, K., "Distributions of noise sources in heated and cold jets: are they different?," *Int. J. Aeroacoust.*, Vol. 9, No. 4&5, 2006, pp. 589-626.

[58]Arndt, R.E.A, Long, D.F., and Glauser, M.N., "The proper orthogonal decomposition of pressure fluctuations surrounding a turbulent jet," *J. Fluid Mech.*, Vol. 340, 1997, pp. 1-33.

[59]Zaman, K.B.M.Q., "Effect of initial boundary-layer state on subsonic jet noise," *AIAA J.*, Vol. 50, No. 8, 2012, pp. 1784-1795.

[60]Brown, G.L. and Roshko, A., "On density effects and large structure in turbulent mixing layers," *J. Fluid Mech.*, Vol. 64, No. 4, 1974, pp. 775-816.

[61]Fleury, V., Bailly, C., Jondeau, E., Michard, M., and Juvé, D., "Space-time correlations in two subsonic jets using dual-PIV measurements," *AIAA J.*, Vol. 46, No. 10, 2008, pp. 2498-2509.

[62]Fleury, V., "Superdirectivit 'e, bruit d'appariement et autres contributions au bruit de jet subsonique," PhD Thesis, No. 2006-18, Ecole Centrale de Lyon, Lyon, France, 2006.

[63]Castelain, T., "Contrôle de jet par microjets impactants. Mesure de bruit rayonné et analyse aérodynamique," PhD Thesis, No. 2006-33, Ecole Centrale de Lyon, Lyon, France, 2006.

[64]Lau, J.C., Morris, P.J., and Fisher, M.J., "Measurements in subsonic and supersonic free jets using a laser velocimeter," *J. Fluid Mech.*, Vol. 93, No. 1, 1979, pp. 1-27.

[65]Uzun, A. and Hussaini, M.Y., "Prediction of noise generated by a round nozzle jet flow using computational aeroacoustics," *J. Comp. Acous.*, Vol. 19, No. 3, 2011, 291-316.